Energy

Volume 3, Issue 3, 297-315.
DOI: 10.3934/energy.2015.3.297
Received date 27 May 2015
Accepted date 22 July 2015
Published date 31 July 2015

http://www.aimspress.com/

Research article

Small scale wind energy harvesting with maximum power tracking

Joaquim Azevedo * and Fábio Mendonça

Centre for Exact Science and Engineering, University of Madeira, Funchal, Portugal

*** Correspondence:** Email: jara@uma.pt; Tel: +351-291-705286.

Abstract: It is well-known that energy harvesting from wind can be used to power remote monitoring systems. There are several studies that use wind energy in small-scale systems, mainly with wind turbine vertical axis. However, there are very few studies with actual implementations of small wind turbines. This paper compares the performance of horizontal and vertical axis wind turbines for energy harvesting on wireless sensor network applications. The problem with the use of wind energy is that most of the time the wind speed is very low, especially at urban areas. Therefore, this work includes a study on the wind speed distribution in an urban environment and proposes a controller to maximize the energy transfer to the storage systems. The generated power is evaluated by simulation and experimentally for different load and wind conditions. The results demonstrate the increase in efficiency of wind generators that use maximum power transfer tracking, even at low wind speeds.

Keywords: energy harvesting; wind energy; horizontal axis wind turbine (HAWT); vertical axis wind turbine (VAWT); maximum power point tracking; simulation; experimental setup

1. Introduction

Many research efforts have been devoted to provide small efficient systems for collecting information from physical world [1–4]. Restrictions of power supply have limited the deployment of large wireless sensor networks. For that reason, these systems require energy harvesting from the environment for long term operation [5–7]. Together with solar and hydro systems, the wind is a renewable energy source mostly used in large-scale systems. Many works have been proposed for solar small-scale energy harvesting [8]. These systems incorporate methods for maximum power point tracking (MPPT) to charge batteries or supercapacitors [7,8]. Several studies suggest the use of wind energy for small-scale systems, mainly with vertical axis wind turbines. Most part of this work

is based on the evaluation of the Savonius turbine [9,11]. However, there are few examples for wind energy harvesting which include the turbine, the generator and a maximum power transfer circuit.

To compare various wind prototypes, it is defined the efficiency of the wind generator as the ratio of the generated output power and the maximum power available from the wind. The system in [12] used a commercial three-bladed turbine (16 cm radius), which provided 200 mW for a wind speed of 5.4 m/s (efficiency of 2.5%). In [13] a piezo electric windmill with blades of 6.5 cm radius produced 5 mW for a wind speed of 4.5 m/s (efficiency of 0.7%). In [14] a vertical axis windturbine (VAWT) six-bladed Savonius (6 cm diameter and 20 cm height) was employed to power wireless sensor networks, providing 45 mW at 5 m/s (efficiency of 0.5%).The work presented in [15] used a wind turbine with a blade radius of 3 cm. The system generated a power of 24 mW for a wind speed of 4.5 m/s (efficiency of 14.9%). The system with MPPT was used to charge a supercapacitor and provided 7.86 mW for a wind speed of 3.62 m/s (efficiency of 9.4%). In [16], horizontal axis windturbines (HAWT) with different number of blades were tested (two, three and six blades with radius of 6.8 cm). The six-bladed turbine provided more energy, producing 136 mW at 5 m/s (efficiency of 12.1%) and 439 mW at 7 m/s (efficiency of 14.2%). The system used a buck regulator to charge batteries of 3.7 V. The charging efficiency was 60% for a wind speed of 7 m/s. The work presented in [17] also studied the number of blades of small HAWT and concluded that turbines with six blades provide more power than those of three blades. For the VAWT system the turbine with two blades produced more power than those of three or six blades. For the wind speed of 5 m/s, the HAWT system with 7.5 cm blade radius produced 243 mW (efficiency of 16.3%) and the VAWT system with the height of 19 cm and a rotor diameter of 6.8 cm produced 83 mW (efficiency of 8.2%).To supply a wireless sensor node, the HAWT system was used to charge batteries of 2.4 V. The system efficiency was 15% at 5 m/s. However, this efficiency drops for other wind speed since the circuit did not use a MPPT algorithm.

Although there are several studies for vertical axis windturbines (typically Savonius), actual implementations of energy harvesting with these systems is difficult to find. More prototypes can be found for horizontal axis windturbines, but there is a lack of studies on some parameters of interest. The first goal of this work is to simulate energy harvesting systems to assist in the development of small-scale wind systems. In this context, it is important to identify the main parameters that affect the performance of the wind energy harvesting system. The power coefficients of two types of turbines will be determined. The efficiency of the wind generator for different load conditions will be evaluated. The systems with MPPT will be compared with those without MPPT. Comparisons between energy harvesting implementations to power wireless sensor networks will also be presented.

2. Materials and Method

Due to the miniaturization of the sensor nodes, energy harvesting systems must also be of small dimension. The development of small-scale wind systems requires the identification of the main parameters that affect the energy generation. A computer model developed to simulate such systems allows its evaluation before its actual implementation. The main components of the wind system are the wind turbine, the generator, the MPPT control circuits and the storage system. In this section the main expressions for simulation and the developed circuits for small-scale wind systems are provided.

2.1. Turbine parameters

The maximum power captured by a wind turbine is given by [18]

$$P_T = C_p P_0 = \frac{1}{2} C_P \rho A v^3 \quad (1)$$

where C_p is the power coefficient of the turbine, P_0 is the maximum available power from the wind, ρ is the air density (typically 1.25 kg/m^3), A is the swept area of the turbine (m^2) and v is the wind speed (m/s). The Betz limit imposes a physical maximum power coefficient of 59.3%. The power coefficient of the wind turbine is determined by the ratio of the shaft power of the turbine and the power available from the wind, $C_p = \omega_m T/P_0$, with ω_m the angular velocity (rad/s) of the turbine and T the aerodynamic torque of the turbine (N·m). The power coefficient may be represented as a function of the tip speed ratio, given by

$$\lambda = \frac{\omega_m R}{v} \quad (2)$$

with R the radius of the turbine rotor.

Figure 1 shows two types of wind turbines developed in this work. HAWT and VAWT systems were evaluated. Three HAWT propeller turbines were tested: three-bladed turbine with 7.5 cm radius, six-bladed turbine with 7.5 cm radius and three-bladed turbine with 15 cm radius. The Savonius VAWT has 25 cm height and a diameter of 12.5 cm. The blades of this turbine were twisted by 180° to provide a surface to start rotating independently of the wind direction.

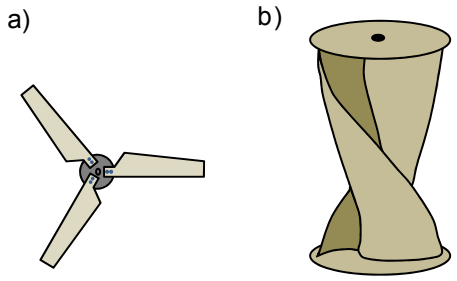

Figure 1.Wind turbines: a) propeller; b) Savonius.

The power coefficient of each turbine was determined using the rope-brake technique to measure the torque [19].

2.2. Generator parameters

The wind turbine was connected to a three-phase permanent magnet synchronous generator (PMSG). Figure 2 shows the model of the generator and the rectifier bridge that converts the alternating current to direct current. Schottky diodes with low on-state voltage drop allow the use of a passive bridge with the advantage that it does not need a control system to maintain the timing of the switch activation required by an active rectifier.

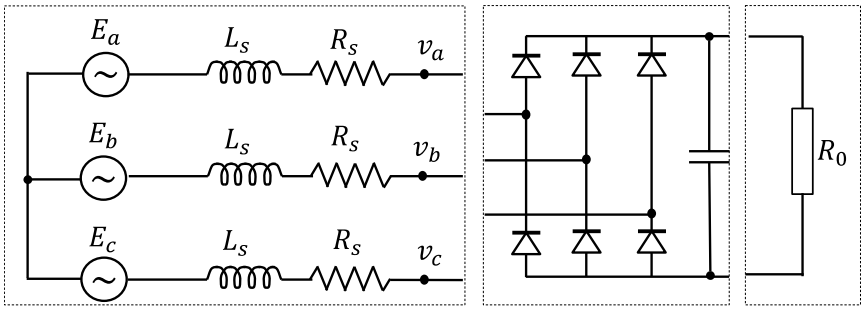

Figure 2.Three-phase generator circuit with rectifier and load.

The generator can be described by [20]

$$\begin{cases} v_a = L_s \dfrac{di_a}{dt} + R_s i_a - E_a \\ v_b = L_s \dfrac{di_b}{dt} + R_s i_b - E_b \\ v_c = L_s \dfrac{di_c}{dt} + R_s i_c - E_c \end{cases} \tag{3}$$

where L_s is the synchronous inductance of each phase, R_s is the phase resistance and E is the maximum induced voltage, given by

$$E_{max} = \frac{4\omega_e k_s N B_m l r}{poles} \tag{4}$$

with $\omega_e=\omega_m poles/2$. K_s is the winding factor, *poles* is the number of poles, N is the number of turns of the stator winding (per phase), B_m *is* the peak flux density (T), l is the axial length of the rotor (m) and r is the radius to the air-gap (m).

The dynamic equation governing the angular velocity of the turbine/generator is [20]

$$\frac{d\omega_m}{dt} = \frac{T_v - T_e - b\omega_m}{J} \tag{5}$$

where b is the coefficient of friction (caused by the generator and the turbine bearings), J is the moment of inertia (kg.m^2), $T_v=P_T/\omega_m$ is the wind torque (N·m) and T_e is the electric torque,

$$T_e = \frac{3IVF_p}{\omega_m} \tag{6}$$

where I is the root mean square (rms) phase current (A), V is the rms phase-to-neutral voltage(V) and F_p the power factor (assumed to be unitary).

Two generators were developed, one for each turbine type. Table 1 shows the main parameters of the generator, with *d* the wire diameter and *a*-*g* the air-gap dimension.

The generator that operates with the propeller turbines was implemented with eight neodymium magnets and six coils of 100 turns with copper wire of 0.4 mm diameter. This generator has a diameter of 5.5 cm and 5 cm height. The generator that operates with the Savonius rotor was implemented with twelve neodymium magnets and nine coils of 135 turns. This generator has a

diameter of 11 cm and 3.5 cm height.

Table 1. Parameters of the generators.

Turbine	*Poles*	Coils	*d* (mm)	*N*	K_s	*l* (cm)	*r* (cm)	B_m (T)	*a-g* (mm)
HAWT	8	6	0.4	100	0.945	4.3	3.3	0.191	3
VAWT	12	9	0.5	135	0.823	5.86	4.86	0.226	3

2.3. Control circuits and simulation

Figure 3 shows the block diagram of the wind system with MPPT control. This model is used for simulation and for the experimental setup. The wind turbine is simulated by equation (5) and provides the mechanical rotation to the generator. The passive rectifier is defined by the on-state voltage drop V_d and by the forward resistance R_d. Schottky diodes (MBRA210LT3G) are used in the experimental setup. The voltage drop is 0.26 V for a forward current of 100 mA. The output voltage of the rectifier bridge is V_s.

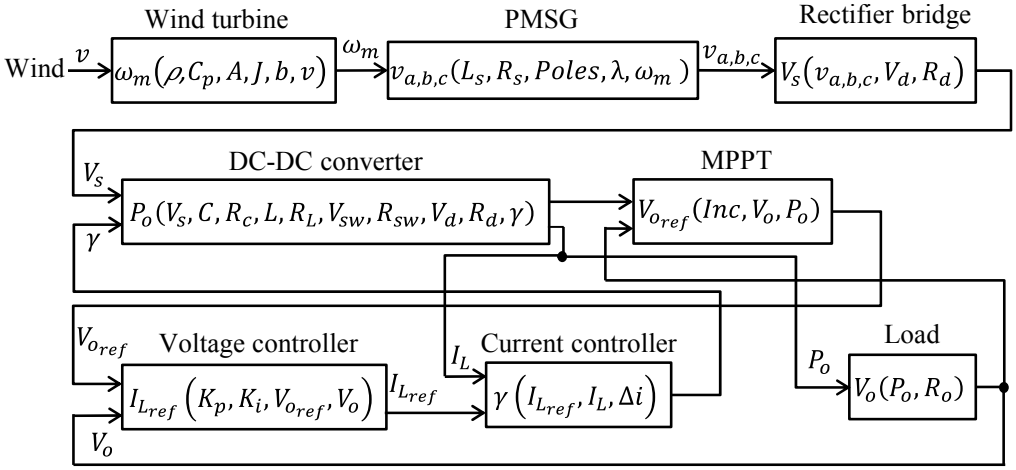

Figure 3.Block diagram of the wind system.

After rectification, a DC-DC converter is used to provide maximum power transfer. Two converter configurations were studied, a boost and a buck-boost [21].Taking into account the required generated voltages, it was decided to use a boost converter, since the buck-boost provides similar results but the circuit is more complicated. In fact, since the buck-boost inverts the output signal in relation to its input, the MOSFET (Metal-Oxide-Semiconductor Field-Effect Transistor) switch is placed at the end of the loop, allowing the emitter to be connected to the source ground. Nevertheless, the microcontroller is powered by the battery, connected at the output of the converter, which requires a driver to keep the control signal. When compared with the boost converter, the loss in efficiency is not compensated by the increase in the output power.

The circuit of the converter is represented in Figure 4. The capacitor *C*is modeled by an ideal capacitance (F) in series with a resistance R_C (Ω), the inductor L (H) has a resistance R_L and the

Schottky diode has an on-state voltage drop V_d and a forward resistance R_d. The MOSFET is controlled by PWM (Pulse Width Modulation). The on-state voltage drop on the MOSFET is V_{sw} and the internal resistance is R_{sw}.

The converter delivers energy to the load R_o, which may be a resistor, a battery or any other system requiring energy. In the present work, a battery is used to supply energy to a wireless sensor node which measures parameters from the environment. A battery was chosen instead of a supercapacitor due to its high storage capacity. The MPPT is implemented using the "perturb and observe" algorithm, with increments on the variable of control given by *Inc*. The output power and voltage are evaluated to determine the reference voltage, V_{oref}. The voltage controller subtracts the voltage on the load to this reference creating the voltage error signal E_v. This signal is compensated by a proportional and integral compensator producing the reference current I_{Lref}. This reference is subtracted to the current on the coil I_L in the current controller, generating the current error. The control signal γ is defined as high (opening the MOSFET switch) if the error is greater than a limit Δi. The control signal is defined as low (closing the switch) if the error is smaller than $-\Delta i$. Otherwise the control signal is not changed.

The control and the MPPT algorithm were implemented in an Arduino Fio microcontroller, as it has low power consumption and is prepared to be integrated with a wireless sensor node XBee [22]. The current on the coil is measured with the current sensor (MAX9929FAUA+) and the voltage on the load is measured directly on its terminals.

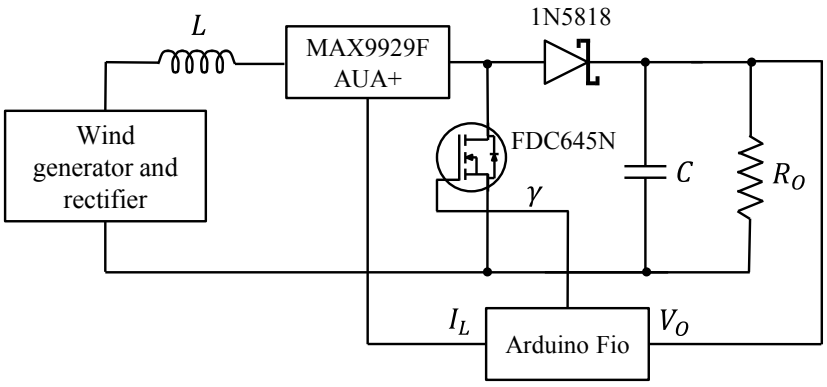

Figure 4.DC-DC boost converter.

The voltage and the current on the load for a boost converter are given by [21]

$$V_o = \frac{V_s}{1-D}$$
$$I_o = (1-D)I_L \tag{7}$$

with D the duty cycle and I_L the current on the coil. The inductance is given by $L = V_sD/(\Delta I_L f)$ and the capacitance $C$is $C=V_oD/(R_o\Delta V_o f)$, where ΔI_L is the current variation on the coil, f is the switching frequency of the converter, V_o is the voltage on the load and ΔV_o is the voltage variation on the capacitor. For design purposes, the maximum voltage elevation should be from 1 to 5 V. Using (7), the maximum value for D is 80%. Considering a current variation of 10% and an average value of I_o of 100 mA (for all loads), from (7) the maximum current variation on the coil is 40 mA. Therefore, if

V_s = 1 V and f = 10 kHz the coil has an inductance of 2 mH. Considering that ΔV_o is 10%, for the lowest load of 5 Ω the capacitance is 160 μF. The resistance of the coil used in the experimental setup is 1 Ωand the equivalent series resistance of the capacitor is 50 mΩ.

The Laplace transform of the dynamic behaviour of the converter is

$$I_L = \frac{1}{sL}\left[V_s - (1-\gamma)V_d - \left(\frac{R_o R_C}{R+R_C}(1-\gamma) + R_L\right)I_L - \frac{R_o}{R_o+R_C}V_C(1-\gamma)\right]i_o = (1-D)i_L \quad (8)$$

$$V_C = \frac{R_o I_L(1-\gamma) - V_C}{sC(R_o+R_C)} \quad (9)$$

where V_d is the voltage drop on the diode (significant for small-scale systems) and γ indicates the switch state (1 if closed or 0 otherwise). The system can perform control of the voltage across the capacitor or it can control the voltage in the capacitor and the current in the coil. The option was for the second case since provides a more stable control. The control circuit uses a proportional and an integral compensator defined by the constants K_p and K_i, where

$$\frac{E_{vc}}{E_v} = K_p\frac{\frac{K_i}{K_p}+s}{s} \quad (10)$$

with E_{vc} the compensated voltage error. The transfer function of the voltage controller is

$$\frac{V_o}{V_{o_{ref}}} = \frac{-\frac{K_p}{CT_d}}{s^2 + \frac{s}{T_d} - \frac{K_p}{CT_d}} \quad (11)$$

using (9) and after manipulation of the expressions, the parameters of the compensator are given by $K_p = -C/(2T_d)$ and $K_i = Kp/(CR_o)$. The system is sampled with a period T to be manipulated with a digital system. The Z transform of the sampled system is

$$E_{vc} = z^{-1}E_{vc} + \left(\frac{TK_i}{2} - K_P\right)z^{-1}E_v + \left(\frac{TK_i}{2} + K_p\right)E_v \quad (12)$$

Simulations in Matlab/Simulink were performed, where the Park transform of the synchronous generator has been already implemented [23].The model of the battery is given in [24].The system is used to charge batteries for wireless sensor nodes and the microcontroller utilized to implement the MPPT control is also used in the application. The microcontroller continuously generates the PWM (Pulse Width Modulation) wave, being in low power consumption mode most of the time and waking up every second to adjust the duty cycle. The current consumption in this mode of operation is 880 μA. Every ten seconds, the microcontroller wakes up the sensor node during 130 ms to measure and transmit data to the gateway and returns to sleep mode to extend the lifetime of the network.

3. Results and Discussion

Several experiments to evaluate the main parameters of the small-scale wind system were

performed. The results are obtained from simulations and experimentally. The study was applied to remote monitoring in urban areas, but the developed systems can be applied to other environments. The availability of higher wind speeds in mountainous regions makes the wind generators a good option for energy harvesting.

3.1. Wind speed

Wind availability was evaluated to determine the amount of energy available for harvesting. Data of wind speeds measured in the years 2012 and 2013 in the top of the University of Madeira was used in this study, which is 175 m above sea level. Figure 5 shows results for the wind speed in May 2013 for a week of data. It may be observed that most of the time the wind speed is very low.

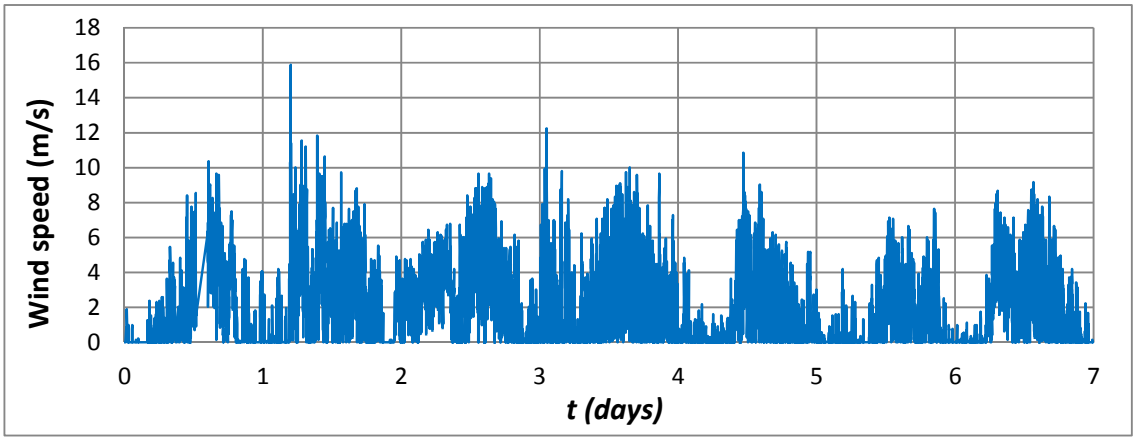

Figure 5. Wind speed for a week of data.

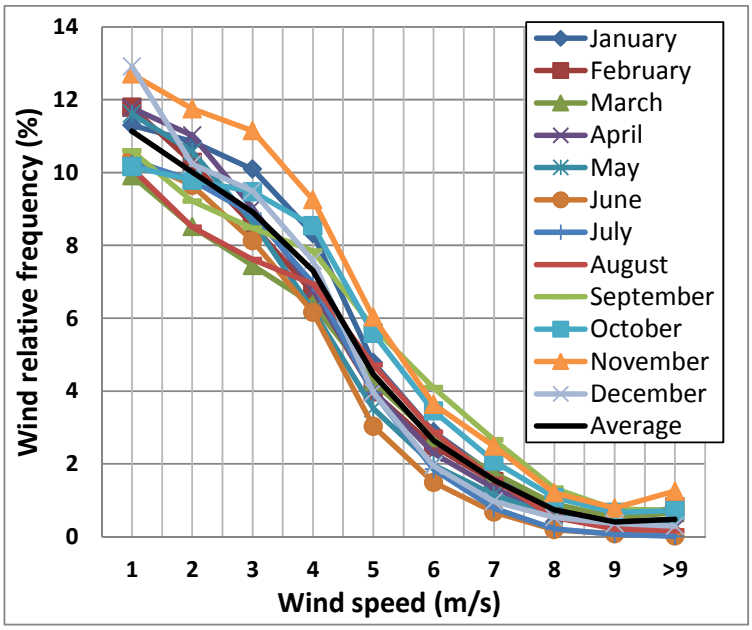

Figure 6. Monthly relative frequency distributions of wind speed.

The relative frequency of wind speed per month was calculated for the considered environment. Figure 6 shows the results. The wind speed is near zero about 50% of the time. This result was removed from the graphs of figure 6 for better visualization of data. The last value represented in the wind speed axis includes the relative frequencies for wind speeds equal or above 10 m/s. The solid line is the annual average of wind speed. The wind frequency decreases considerably with increasing wind speed. Wind speed is around 2 m/s in about 10% of the time and is around 5 m/s in about 5% of the time. Speeds above 8 m/s only occur in 2% of the time.

3.2. Power coefficients of wind turbines

The power coefficient is a very important parameter of a wind turbine. In [25], it is mentioned that the efficiency of small blades can be less than 20%. Horizontal and vertical axis small wind turbines were tested in order to perform a comparison with large-scale wind turbines. Figure 7 shows the power coefficients of three-bladed horizontal axis turbines for different radius.

Large-scale three-bladed turbines can have power coefficients above 40% [26]. This is represented in figure 7 by a solid line. The solidity of these turbines is 0.035. The dashed line is the power coefficient measured for a turbine with a smaller radius [27]. In this case the value of C_p is lower. The results represented by triangles, squares and dots were obtained in this work for small turbines. It may be noticed that the power coefficient decreases with the radius of the turbine. The tip speed ratio decreases due to the increasing in solidity (0.22 for 5 cm radius, 0.17 for 7.5 cm radius and 0.12 for 15 cm). The experiments demonstrate that the angular velocity of the turbine increases linearly with the wind speed. Smaller turbines provide higher angular velocities for the same wind speed. However, the torque increases more quickly with the turbine diameter, resulting in a higher power coefficient for turbines with higher radius.

Figure 8 shows the power coefficient as a function of the wind speed for the various tested turbines. The six-bladed HAWT have a higher C_p (26.5%) than the three-bladed (25.5%), as obtained by other works. These turbines have a maximum power coefficient for wind speeds around 5 m/s. The efficiency of propeller turbines with larger radius decreases more quickly with wind speed than for turbines with smaller radius. The turbine of 5 cm radius has a low performance since in this case the bearings impose a greater influence.

The VAWT system has a maximum C_p of 10.2% (dashed line with dots), but this parameter has a smaller variation with the wind speed compared with the horizontal axis turbines. In the following sections, the six-bladed horizontal axis turbine and the vertical axis wind turbine are used in the studies of power generation.

3.3. Power generation for different loads

Simulated and experimental results for both wind turbines and for different load resistances were obtained. The moment of inertia of the HAWT system was calculated using the expression given in [28] and the moment of inertia of the VAWT system was calculated with the expression developed in [29].Considering the information given in [30], the bearing constants are in the interval 8×10^{-4} to 12×10^{-4}. The turbine shaft is supported by two bearings. A comparison between simulated and experimental results has shown that the coefficient of friction varies with the wind speed and load. An empirical expression was obtained from the results of the HAWT system, giving

$$b = 0.0019 - 0.00055\ln(v) - 0.000025\ln(R_0) \quad (13)$$

From simulation, it was found the generator efficiency is strongly dependent on the coefficient of friction of the bearings. Variations of the moment of inertia in (5) affects the time required for the wind generator to reach the final value.

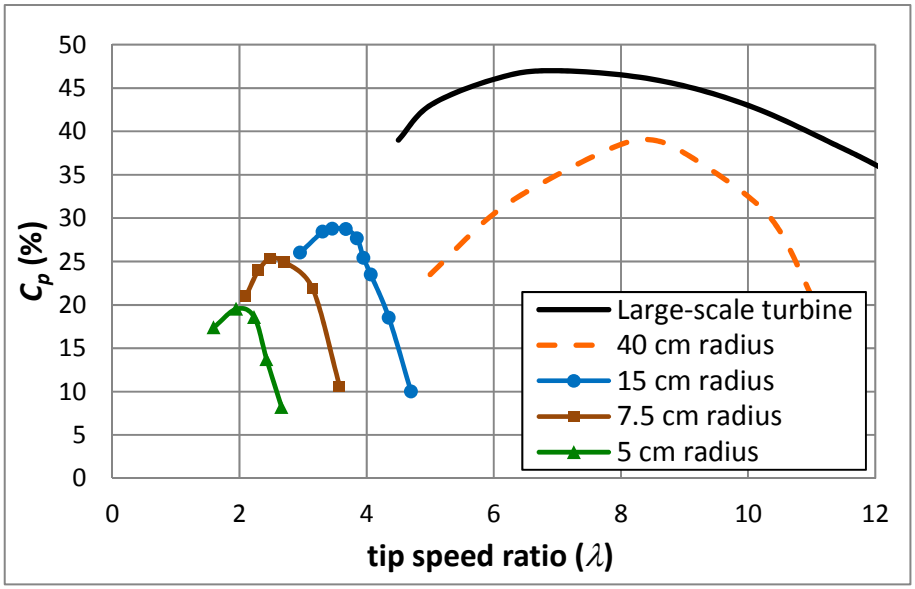

Figure 7. Power coefficients of three-bladed horizontal axis wind turbines.

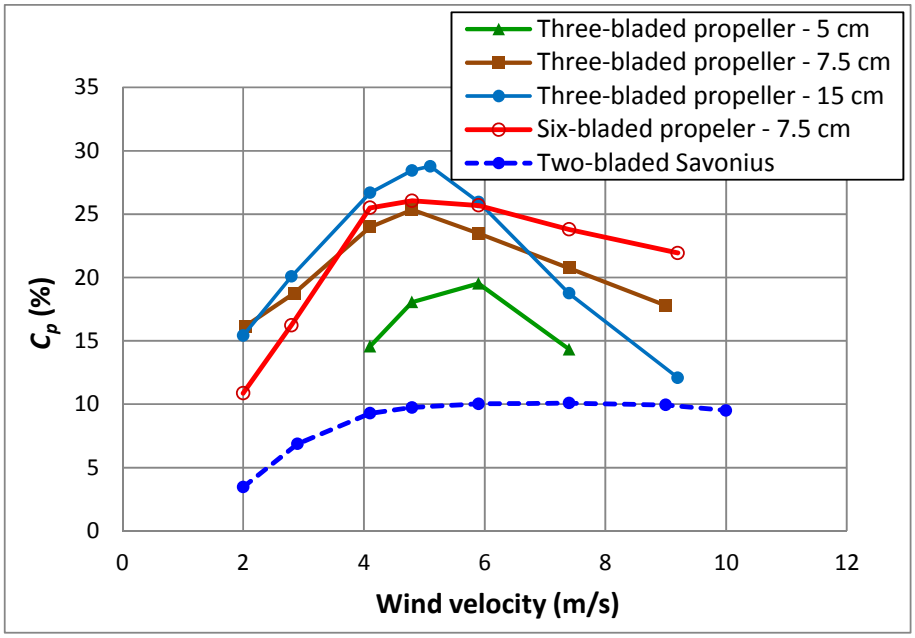

Figure 8. Power coefficients of the developed wind turbines.

Figure 9 shows the output power of the systems without MPPT for different wind speeds. Figure 9a) and figure 9b) are results for the horizontal axis turbine and Figure 9c) and figure 9d) are

results for the vertical axis turbine. Solid lines are experimental data (E) and dashed lines are results obtained from simulation (S). The maximum power transfer occurs for loads between 10 and 66 Ωfor the range of wind speeds used in the measurements. Higher wind speeds correspond to lower load resistances.

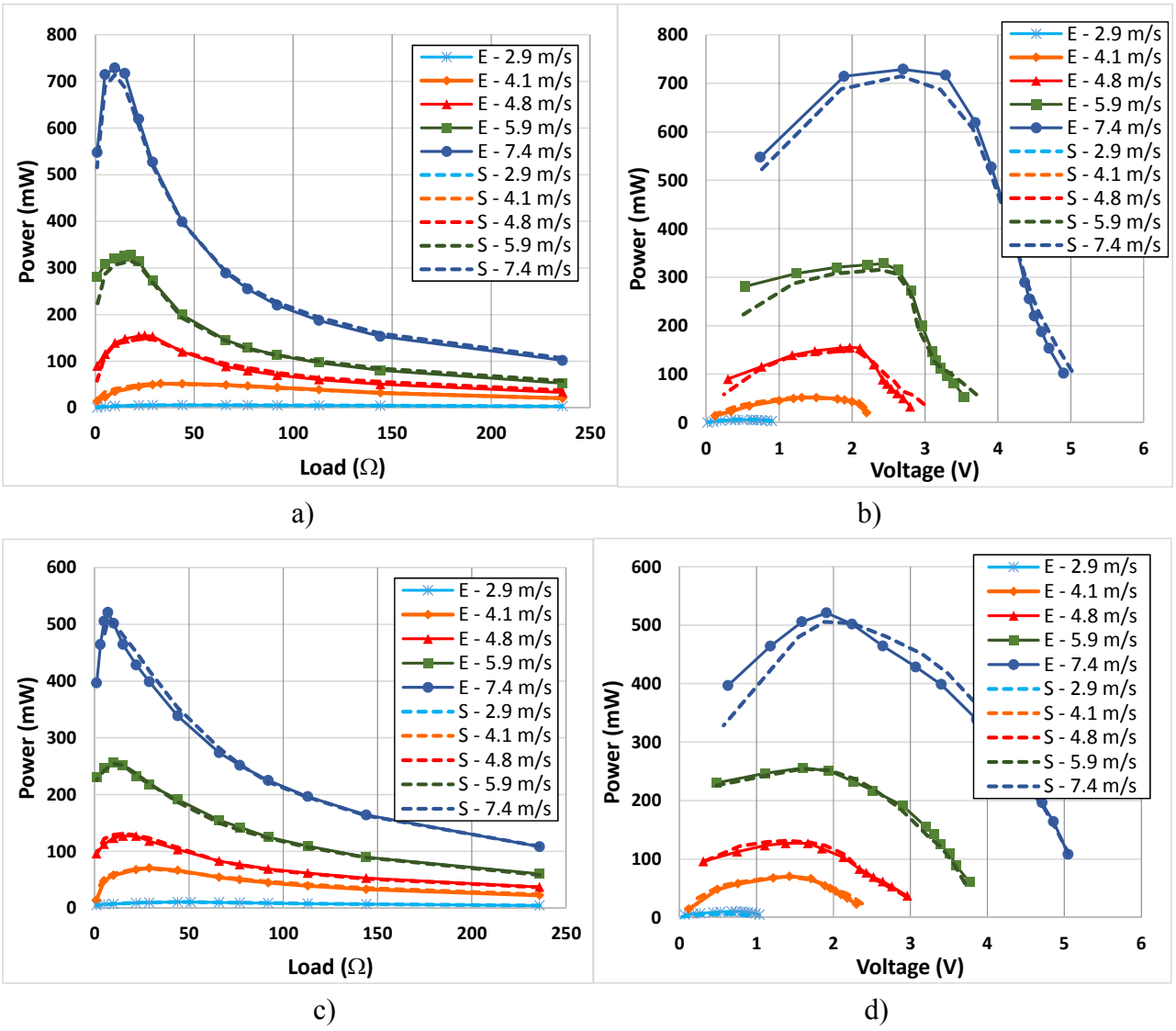

Figure 9. Output power: a) as a function of load resistances for HAWT; b) as a function of generated voltage for HAWT; c) as a function of load resistances for VAWT; d) as a function of generated voltage for VAWT.

Figure 9b) and figure 9d) show results for the output power as a function of the generated voltage. The efficiency of the passive rectifier bridge is between 60% for $v = 2.5$ m/s and 84% for $v = 7.5$ m/s. The efficiency of the generator of the HAWT system is between 20% for $v = 2.5$ m/s and 83% for $v = 7.5$ m/s. For the VAWT system the efficiency of the generator is between 47% for $v = 2.5$ m/s and 84% for $v = 7.5$ m/s.

Figure 10 shows the total efficiency of the system (this efficiency includes power coefficient, generator efficiency and rectifier efficiency). The HAWT system provides higher efficiencies except

for low wind speeds. However, in this case it is required a system that orientates the turbine to the wind direction. The efficiency of the VAWT system varies less with the wind speed.

From data of figure 6, it was calculated the annual mean of wind speed. The result was 1.5 m/s. If this wind speed were used in the calculation of the mean generated power, the result would be 0.2 mW for the HWAT system and 0.4 mW for the VAWT system. However, high wind speeds provide higher values of energy harvesting. Considering the average relative frequency, the average generated power is 53 mW for the HWAT system and 42 mW for the VAWT system. This power is enough to supply energy to a wireless sensor node consuming few tens of milliwatts.

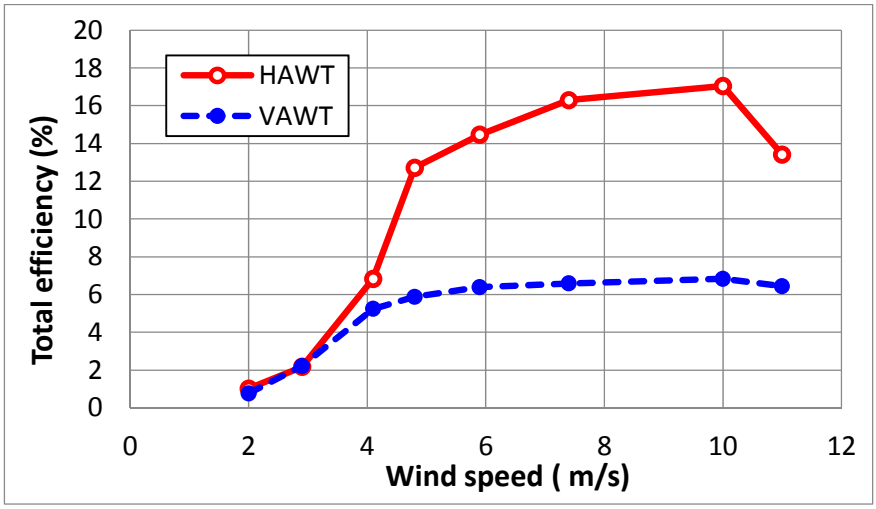

Figure 10.Total efficiency for HAWT and VAWT systems.

3.4. Power transfer

The systems with MPPT were evaluated and compared to those without control. Figure 11 shows the results for the HAWT system considering four wind speeds. The generated output power is represented as a function of the generated voltage, since the energy is used to charge batteries in typical applications. The dashed lines are results obtained from simulation and the solid lines are experimental results. There is a good correlation between both results. Therefore, the model can be used to evaluate the parameters of the wind system that influence the energy generation.

The lines defined by small squares are the output powers for the wind system with MPPT. It may be observed that MPPT control is very important for low wind speeds. The generated power of the system with MPPT is higher than that of the system without MPPT for all generated voltages for wind speeds below 4 m/s. Taking into account data of figure 6, the wind speed is below 4 m/s for about 90% of the time. The system operating above 6 m/s has better results if the DC-DC control is not used for lower generated voltages. For 6 m/s the transition occurs at 3 V and for 7.5 m/s at 4.2 V. However, it is important to note the energy harvesting system always requires the converter as it allows controlling the flow of current to the battery. The wind speed is above 6 m/s for about 5.8 % of the time (figure 6).

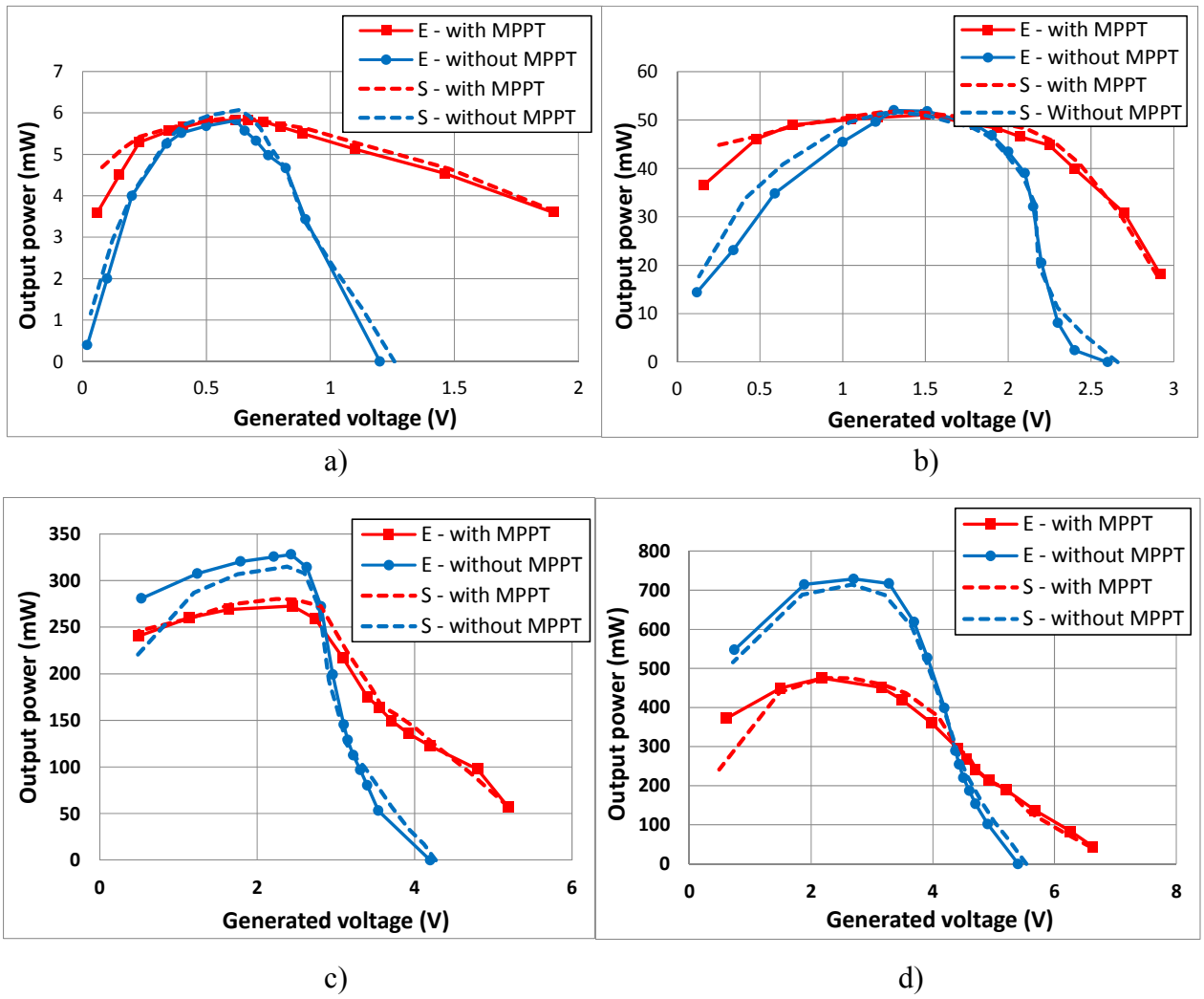

Figure 11. Output power as a function generated voltage for the HAWT system: a) 2.9 m/s; b) 4.1 m/s; c) 5.9 m/s; d) 7.4 m/s.

In figure 12 is represented the efficiency of the DC-DC. This efficiency is measured as the ratio of the output power of the DC-DC converter to its input power. The efficiency is above 60% for wind velocities above 5 m/s. The converter provides lower efficiencies for lower wind speeds. However, in this case the generated power is near the one of the maximum transfer for a wide range of loads. The quality of the coil, the equivalent series resistance of the capacitor and the voltage drop in the diode affects the efficiency of the converter. This influence was evaluated by simulation. The results demonstrate that high efficiencies are obtained by the use of components with low losses. Nevertheless, it should be considered that a coil and a capacitor with low losses require larger dimensions.

Figure 13 shows the results for the VAWT system. The conclusions about the performance of the system with MPPT are similar to those of HAWT system. However, the VAWT system provides more power for wind speeds below 4 m/s.

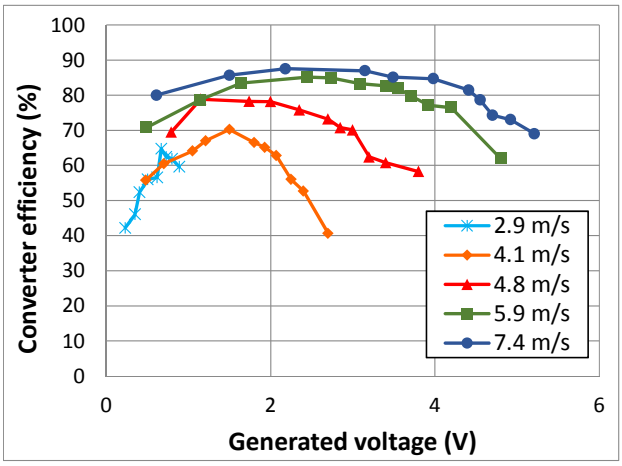

Figure 12. Efficiency of the DC-DC converter.

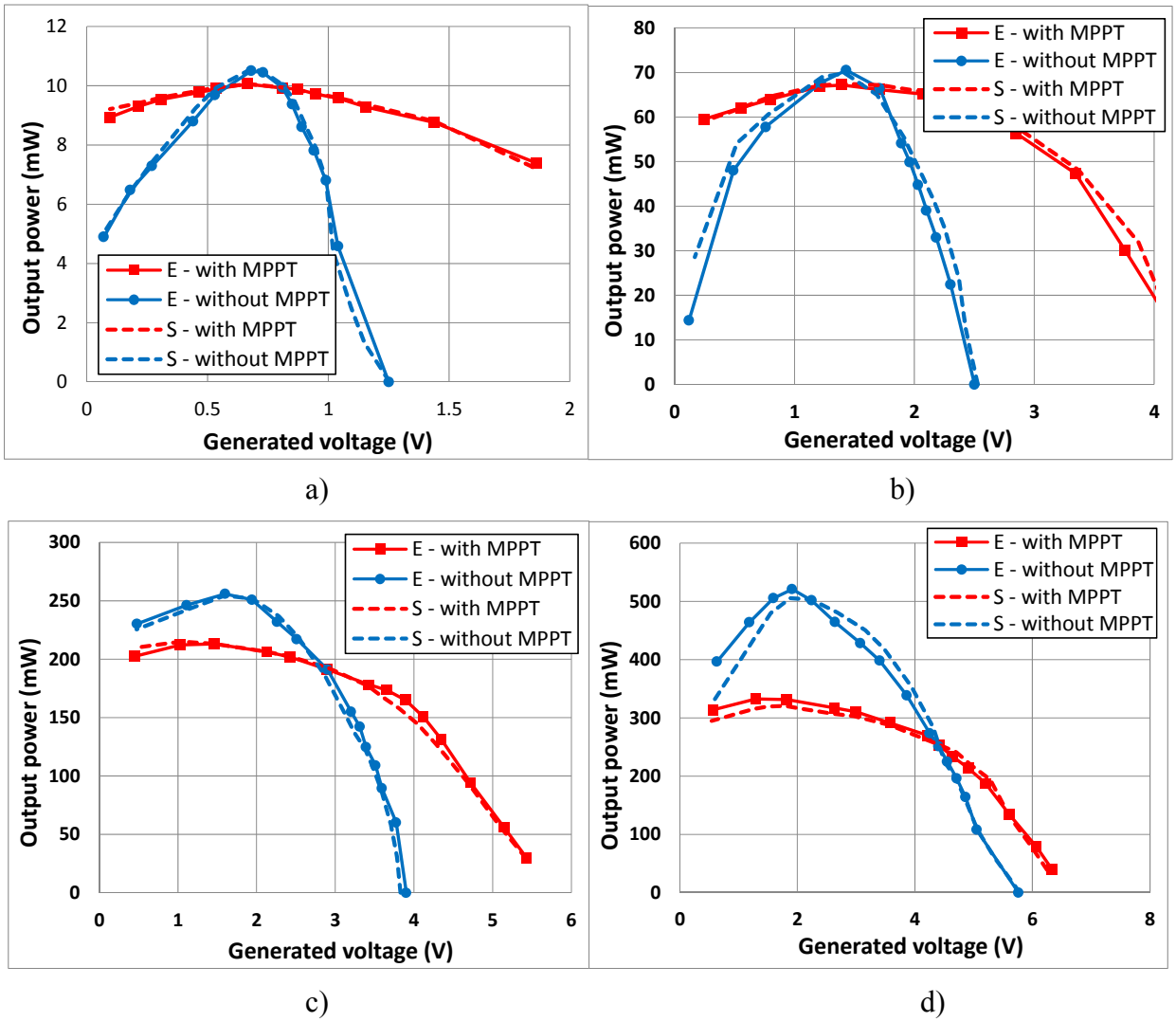

Figure 13. Output power as a function generated voltage for VAWT system: a) 2.9 m/s; b) 4.1 m/s; c) 5.9 m/s; d) 7.4 m/s.

3.5. Environment monitoring with energy harvesting

A wireless sensor network with Xbee/Zigbee sensor nodes is used to monitor parameters of the environment. The XBee operates with voltages between 2.1 V and 3.6 V. The operating current consumption at 3.3 V is 40 mA and the power-down current is below 1 μA. Typically, a pair of AA batteries is used to supply energy to these systems. The microcontroller Arduino Fio operates at 3.3 V and the input voltage range from 3.35 V to 12 V. An integrated controller allows charging lithium batteries of 3.7 V with an input voltage range from 3.7 V to 7 V. Three types of battery voltages were evaluated: two AA batteries in series to give 2.4 V; a lithium battery of 3.7 V; four AA batteries in series to give 4.8 V.

The developed systems were applied to charge the mentioned batteries. The initial voltage of the batteries was near the nominal for a better comparison between systems. Table 2 shows the output power of the HAWT system for several wind speeds. For the battery of 2.4 V the system with MPPT produces high efficiencies at low wind speeds. The system without MPPT cannot charge this battery for wind speeds below 4 m/s. The system with MPPT can also charge the battery of 3.7 V with very good efficiencies. As for the previous case, the efficiency decreases with the increasing of the wind speed. The system without MPPT only charges the 3.7 V battery for wind speeds above 5.7 m/s. Wind speeds below 3 m/s cannot charge the battery of 4.8 V for the system with MPPT. For the system without MPPT only very high wind speeds permit to charge this battery.

Table 2. Output power of the HAWT system when charging different batteries.

	2.4 V		**3.7 V**		**4.8 V**	
v (m/s)	With MPPT (mW)	Without MPPT (mW)	With MPPT (mW)	Without MPPT (mW)	With MPPT (mW)	Without MPPT (mW)
2.9	8	0	4	0	0	0
4.1	40	8	27	0	5	0
4.8	84	84	67	0	41	0
5.9	190	134	142	4	93	0
7.4	358	348	264	133	193	7

A similar study was also applied to the VAWT system, being the results on table 3.The generated power of the VAWT is lower than that of the HAWT for wind speed above 5 m/s.

The wind systems were installed in the studied environment for energy harvesting. The sensor nodes send data of temperature and humidity with a sampling period of 10 seconds. The power consumption of the monitoring system is 5.7 mW. The wind generators are used to charge batteries of 3.7 V. Figure 14 shows the harvested power for one day of operation. In figure 14a) is represented the wind speed and in figure 14b) is the generated power for HAWT and VAWT systems. The average wind speed is 2.2 m/s. In the study performed previously it was found that the HAWT system is more efficient and produces more power than the VAWT, mainly for high wind velocities. However, from the results of figure 14b) it may be observed that the horizontal wind generator produces less power than the vertical wind generator. The reason is that the wind was constantly

changing direction, which forced the HAWT system to reorient its direction. The average power of the HAWT system is 6.8 mW and of the VAWT is 26.9 mW. These values are enough to maintain the batteries charged.

Table 3. Output power of the VAWT system when charging different batteries.

	2.4 V		3.7 V		4.8 V	
v (m/s)	With MPPT (mW)	Without MPPT (mW)	With MPPT (mW)	Without MPPT (mW)	With MPPT (mW)	Without MPPT (mW)
2.9	17	0	8	0	0	0
4.1	54	22	38	0	6	0
4.8	83	46	64	0	36	0
5.9	165	152	138	4	74	0
7.4	294	315	231	130	159	2

4. Conclusion

In this work implementations of wind systems to power supply wireless sensor nodes for remote sensing were presented. The power coefficients of small-scale horizontal axis wind turbine were determined. The results have shown efficiencies between 10% and 30% for radius of the turbine in the range from 5 cm to 15 cm. This parameter is dependent on the wind speed. Small-scale vertical axis turbines provide lower efficiencies, but the power coefficient varies less with the wind speed. A study of wind in an urban environment has demonstrated that the wind speed is below 5 m/s most of the time. A DC-DC converter with MPPT to provide maximum power transfer was implemented. The system was able to charge typical batteries used to supply sensor nodes. Without such system no current flows to the batteries at some lower wind speeds. A computer model to evaluate the main parameters of a wind system was developed. The model considers parameters of the turbine/generator, converter and load/battery. Simulations have demonstrated that the generated power by small-scale wind systems is strongly affected by the bearings that support the turbine shaft. It was also observed that the quality of the coil and of the capacitor used in the converter affects its efficiency. The actual implementation of the circuit requires a compromise between quality and size of the components. The HAWT and VAWT systems were installed in the actual environment for energy harvesting. The efficiency of HAWT system can be lower than expected due to the need of the turbine to follow the wind direction if the wind speed and direction change constantly.

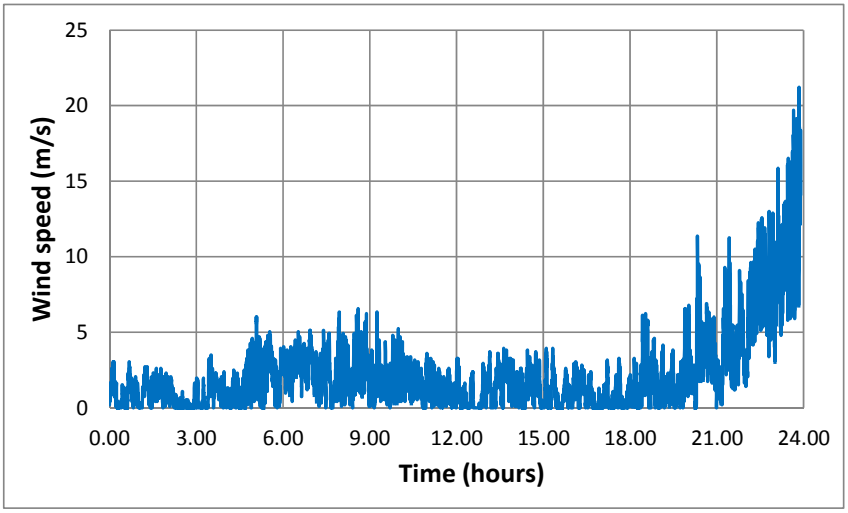

a)

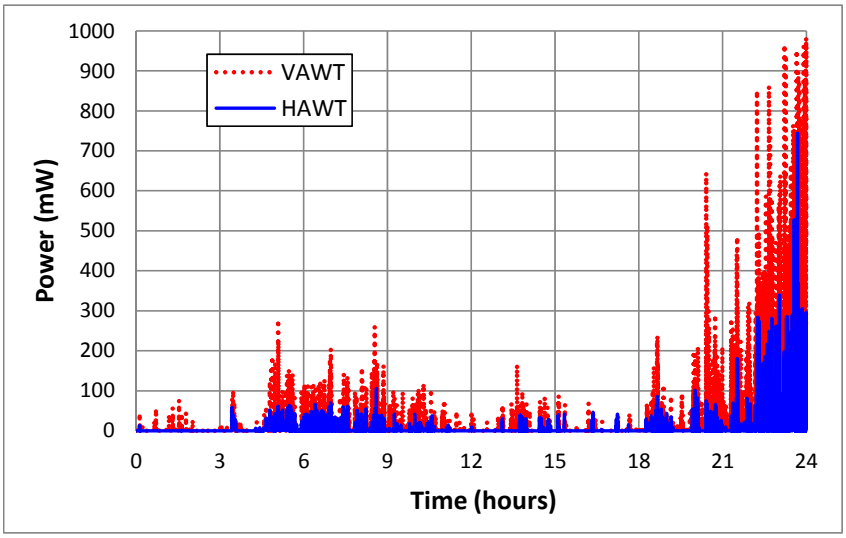

b)

Figure 14. Harvesting energy: a) wind speed; b) power into the battery.

Acknowledgments

This work was supported by the CCM research unit through the program PEst-OE/MAT/UI0219/2014.The authors wish to thank to Filipe Santos for his support to this work.

Conflict of Interest

All authors declare no conflicts of interest in this paper.

References

1. Akyildiz IF, Su W, Sankarasubramaniam Y, et al. (2002) Wireless sensor networks: a survey. *Comput Netw* 38: 393–422.

2. Anastasi G, Conti M, Di Francesco M (2009) Extending the lifetime of wireless sensor networks through adaptive sleep. *IEEE T Ind Inform* 5: 351–365.
3. Oliveira L, Rodrigues J (2011) Wireless sensor networks: a survey on environmental monitoring. *J Commun* 6: 143–151.
4. Pantazis N, Nikolidakis S, Vergados D (2013) Energy-efficient routing protocols in wireless sensor networks: a survey. *IEEE Commun Surv Tut* 15: 551–591.
5. Niyato D, Hossain E, Rashid M, et al. (2007) Wireless sensor networks with energy harvesting technologies: a game-theoretic approach to optimal energy management. *IEEE Wirel Commun* 14: 90–96.
6. Tan Y, Panda S (2011) Self-autonomous wireless sensor nodes with wind energy harvesting for remote sensing of wind-driven wildfire spread. *IEEE T Instrum Meas* 60: 1367–1377.
7. Wan Z, Tan Y, Yuen C (2011) Review on energy harvesting and energy management for sustainable wireless sensor networks. *Proceedings of the IEEE International Conference on Communication Technology* 2011: 362–367.
8. Simjee F, Chou P (2008) Efficient charging of supercapacitors for extended lifetime of wireless sensor nodes. *IEEE T Power Electr* 23: 1526–1536.
9. Saha U, Thotla S, Maity D (2008) Optimum design configuration of Savonius rotor through wind tunnel experiments. *J Wind Eng Ind Aerod* 96: 1359–1375.
10. Kamoji M, Kedare A, Prabhu S (2009) Experimental investigations on single stage modified Savonius rotor. *Appl Energ* 86: 1064–1073.
11. Bhuyan S, Biswas A (2014)Investigations on self-starting and performance characteristics of simple H and hybrid H-Savonius vertical axis wind rotors. *Energ Convers Manage* 87: 859–867.
12. Park C, Chou P (2006) AmbiMax: Autonomous Energy Harvesting Platform for Multi-Supply Wireless Sensor Nodes. *Annual IEEE Communications Society on Sensor and Ad Hoc Communications and Networks* 2006: 168–177.
13. Myers R, Vickers M, Kim H, et al. (2007) Small scale windmill. *Appl Phys Lett* 90: 054106.
14. Morais R, Matos S, Fernandes M, et al.(2008) Sun, wind and water flow as energy supply for small stationary data acquisition platforms. *Comput Electron Agr* 64: 120–132.
15. Tan Y, Panda S (2011) Optimized Wind Energy Harvesting System Using Resistance Emulator and Active Rectifier for Wireless Sensor Nodes. *IEEE T Power Electron* 26: 38–50.
16. Park J, Jung H, Jo H, et al. (2012) Feasibility Study of Micro-Wind Turbines for Powering Wireless Sensors on a Cable-Stayed Bridge. *MDPI: Energies* 5: 3450–3464.
17. Azevedo JAR, Santos FES (2012) Energy harvesting from wind and water for autonomous wireless sensor nodes. *IET Circ Device Syst* 6: 413–420.
18. Wilson RE, Lissaman PBS (1974) Applied aerodynamics of wind power machines. Research Applied to National Needs, Oregon State University.
19. Singh S (2009) *Theory of Machines*, 2 Eds., Singapore: Pearson Education.
20. Umans S, Fitzgerald A, Kingsley C (2014.) *Electric Machinery*, 7th Eds., New York, USA: McGraw Hill Higher Education.
21. Hart DW (2014) *Power Electronics*. New York, USA: McGraw Hill Higher Education.
22. XBee. Available from: http://www.digi.com/XBee.
23. MathWorks, Permanent Magnet Synchronous Motor. Available from: http://www.mathworks.com/help/physmod/sps/ref/permanentmagnetsynchronousmotor.html.

24. MathWorks, Battery. Available from: http://www.mathworks.com/help/physmod/sps/powersys/ref/battery.html;jsessionid=e65abbf4e8de0c995236e4914c0e.
25. Federspiel C, Chen I (2003) Air-powered Sensor. *Proc IEEE Sensor* 1: 22–25.
26. Burton T, Sharpe D, Jenkins N, et al. (2001) *Wind Energy Handbook*, Chichester, USA: John Wiley and Sons.
27. Velázquez M, Carmen M, Francis J, et al. (2014) Design and Experimentation of a 1 MW Horizontal Axis Wind Turbine. *J Power Energ Eng* 2: 9–16.
28. Muyeen S, Tamura J, Murata T (2009) Stability Augmentation of a Grid-connected Wind Farm. London, UK: Springer-Verlag.
29. Ali MH (2013) Experimental Comparison Study for Savonius Wind Turbine of Two & Three Blades At Low Wind Speed. *Int J Mod Eng Res* 6: 2978–2986.
30. Koyo, Ball and Roller Bearings, JTEKT North America Corporation, Available from: http://www.koyousa.com/assets/ce/Documents/(B2001E-5a)%20Ball%20and%20Roller%20Bearing%20Catalog%20-%20Technical%20Section.pdf.